A&A 530, A72 (2011)
DOI: 10.1051/0004-6361/201116580

Astronomy & Astrophysics

A study of the association of *Fermi* sources with massive young galactic objects⋆

P. Munar-Adrover[1], J. M. Paredes[1], and G. E. Romero[2,3]

[1] Departament d'Astronomia i Meteorologia, Institut de Ciències del Cosmos (ICC), Universitat de Barcelona (IEEC-UB), Martí i Franquès 1, 08028 Barcelona, Spain
e-mail: pmunar@am.ub.es
[2] Instituto Argentino de Radioastronomía, CONICET, C.C.5, Villa Elisa, 1894, Argentina
e-mail: romero@iar.unlp.edu.ar
[3] Facultat de Ciencias Astronómicas y Geofísicas, Universidad Nacional de La Plata, Paseo del Bosque, La Plata 1900, Argentina

Received 25 January 2011 / Accepted 21 March 2011

ABSTRACT

Massive protostars have associated bipolar outflows that can produce strong shocks when they interact with the surrounding medium. At these shocks, particles can be accelerated up to relativistic energies. Relativistic electrons and protons can then produce gamma-ray emission, as some theoretical models predict. To identify young galactic objects that may emit gamma rays, we crossed the *Fermi* First Year Catalog with some catalogs of known massive young stellar objects (MYSOs), early type stars, and OB associations, and we implemented Monte Carlo simulations to find the probability of chance coincidences. We obtained a list of massive MYSOs that are spatially coincident with *Fermi* sources. Our results indicate that ∼70% of these candidates should be gamma-ray sources with a confidence of $\sim 5\sigma$. We studied the coincidences one by one to check the viability of these young sources as potential counterparts to *Fermi* sources and made a short list of best targets for new detailed multifrequency observations. The results for other type of young galactic objects are not conclusive.

Key words. stars: early-type – gamma rays: stars – ISM: jets and outflows

1. Introduction

Recently, massive young stellar objects (MYSOs) have been suggested as gamma-ray sources (Araudo et al. 2007; Romero 2008; Bosch-Ramon et al. 2010). Massive stars are formed in dense cores of cold clouds. The processes that take place during the formation of the star are mostly unknown. It is clear, however, that the formation of massive stars involves outflows (Garay & Lizano 1999; Reipurth & Bally 2001). The accumulation of material around the core of the cloud would generate a massive protostar that starts to accrete material from the environment. The accretion is expected to have angular momentum that leads to the formation of an accretion disk. The rotation would twist the strong magnetic fields present in the progenitor cloud around the disk, where a magnetic tower can be formed, giving rise to collimated outflows or jets, as simulations predict (Banerjee & Pudritz 2006, 2007). The observational evidence of outflows comes from methanol masers and from direct detection of thermal radio jets. These jets propagate along distances in a fraction of a parsec (Martí et al. 1993). At the jet termination region, interaction with the external medium creates two shocks: a bow shock moving in the interstellar medium (ISM) and a reverse shock in the jet. These shocks can accelerate particles that, in turn, can produce gamma rays trough inverse Compton (IC) scattering of infrared (IR) photons, relativistic Bremsstrahlung, or inelastic proton-proton collisions, if protons are accelerated as well. In some cases non thermal radio lobes and jets have been observed, indicating the presence of relativistic electrons that produce synchrotron radiation (Garay et al. 2003; Carrasco-González et al. 2010).

Other possible scenarios have been suggested for the gamma-ray production involving young stars, such as the case of the massive stars with strong winds. In this scenario, gamma-rays could be produced in the interaction between the supersonic winds and the ISM. The terminal shock can accelerate particles and ions up to high energies, which might interact with the ambient matter producing gamma-rays. Whereas the luminosity produced by a single massive star wind should be low, collective effects might be important (Torres et al. 2004).

Gamma-rays can also be produced in the wind interaction region of a WR+OB binary system (Benaglia & Romero 2003). In this case, the acceleration region is between the two components of the binary system and is exposed to strong photon fields where IC cooling of the electrons can generate a significant amount of high-energy (HE) non thermal emission. A source of this class, η-Carinae, has been recently detected at $E > 100$ MeV by *AGILE* (Tavani et al. 2009).

Of-type stars have strong winds with velocities higher than the escape velocity, which implies a strong mass loss rate (10^{-6}–10^{-5} $M_\odot$ yr^{-1}). The action of this wind in the ISM can create hot gas bubbles with expanding boundaries of swept-up material, which might produce gamma rays in a similar way to the case of WR stars. The case of gamma-ray emission in Of-type stars has been discussed in the past, e.g. by Voelk & Forman (1982). The predicted luminosity, however, is still below the current sensitivity of gamma-ray instruments.

⋆ Table 6 is available in electronic form at http://www.aanda.org

Finally, OB associations are tracers of a number of galactic objects that can produce gamma rays, such as neutron stars, massive stars with strong winds, young stellar objects (YSOs), etc. They are also thought to be places where acceleration of a significant fraction of galactic cosmic rays (CRs) might occur (e.g. Binns et al. 2008).

The aim of this work is to find evidence supporting the presence of HE emission coming from massive YSOs and other young galactic sources. To attain this goal we study the spatial coincidence between gamma-ray sources detected by *Fermi* and samples of young objects, such as YSOs, WR stars, Of-type stars, and OB associations. We also estimate the probability of chance coincidences by using Monte Carlo simulations, and we provide a list of counterpart candidates of the gamma-ray sources.

2. Cross-correlation of the First *Fermi* Catalog with massive young galactic objects

There is not observational evidence of any YSO emitting gamma-rays so far. The new generation of gamma-ray telescopes, like *Fermi*, will make it possible to reach the necessary sensitivity level to detect these faint gamma-ray sources soon, in case the predictions were right. To identify those young objects that might be emitting gamma rays, we first took the recently published First *Fermi* Catalog (Abdo et al. 2010) by the *Fermi* Collaboration and we excluded all known firm identifications, getting a list of 1392 sources. Then we crossed this list with catalogs of confirmed and well characterized YSOs and other type of young stars. We also did a Monte Carlo study to determine the probability of pure chance coincidences between the crossed catalogs.

2.1. Catalogs

The catalogs used in this study are listed in Table 1. Here we describe each one in more detail.

The *Fermi Large Area Telescope* First Catalog (Abdo et al. 2010) contains the detected sources during the first 11 months of the science phase of the mission, which began on 2008 August 4. This catalog contains 1451 gamma-ray sources detected and characterized in the 100 MeV to 100 GeV range with a typical position uncertainty of ∼6′. After excluding the firm identifications from the original sample, we get 1392 sources. Most of them are located on the Galactic plane (see Fig. 1).

The Red *MSX* Source (RMS) survey is an ongoing multi wavelength (from radio to infrared) observational program with the objective of providing a well-selected sample of MYSOs in the entire Galaxy (Urquhart et al. 2008). About ∼2000 MYSO candidates have been identified by comparing the colors of *MSX* and 2MASS point sources (at 8, 12, 14, and 23 μm) with those of well known MYSOs. The survey also uses high-resolution radio continuum observations at 6 cm obtained with the VLA in the northern hemisphere and at 3.6 cm and 6 cm with ATCA in the southern hemisphere. They help to distinguish between genuine MYSOs and other types of objects, such as ultracompact HII regions, evolved stars, or planetary nebulae, which contaminate the sample. In addition to these targeted observations, archival data of a previous VLA survey of the inner Galaxy were used. This ongoing program has provided a sample of 637 well-identified MYSOs until now, which were used in our work.

The VIIth catalog of Population I WR stars (van der Hucht 2001) contains 227 stars, with spectral types and *bv* photometry. In recent years, the number of WR stars has increased in 71 new stars, respect to the VIth catalog and the coordinates have also been improved. The position uncertainty is close to a fraction of an arcsecond.

The catalog of Of-type stars is the one of Cruz-González et al. (1974), which contains 664 stars. The catalog provides m_v, $B - V$, spectral type, radial velocity, radial component of the peculiar velocity, possible multiplicity of the object, and other characteristics for each source. The typical uncertainty in the star position is ∼1′.

Finally, the catalog of OB associations is the one by Mel'Nik & Efremov (1995). This catalog contains 88 associations and provides distances to the association, number of stars, and size of the association along the Galactic latitude and longitude axes. The typical value of the size is ∼20−30 pc.

2.2. Spatial coincidences

We crossed the *Fermi* catalog with the catalogs of young galactic objects mentioned above. We calculated the distance between two sources using the statistical parameter S (Allington-Smith et al. 1982):

$$S = \sqrt{\frac{(\Delta\alpha \cos\delta)^2}{\sigma_{i_\alpha}^2 + \sigma_{j_\alpha}^2} + \frac{\Delta\delta^2}{\sigma_{i_\delta}^2 + \sigma_{j_\delta}^2}}$$

where $\Delta\alpha$ and $\Delta\delta$ are the difference between the right ascension and the declination of the two compared sources, respectively, σ_{a_b} is the uncertainty in the position of the source, and (i, j) represent the two sources. The error in the position of the *Fermi* sources is taken as the 95% confidence ellipse. The error in the position of the other compared sources is the precision in the coordinates for YSOs, WR stars and Of-type stars, and the angular size of the association in the case of OB associations. If S is lower than or equal to the unit, it means that the source position (YSO, WR, Of-type, or OB associations) is inside the 95% uncertainty ellipse of the *Fermi* source, within its own position uncertainty, and that case is considered to be a coincidence. Massive YSO and protostar are point-like objects compared with the confidence contours of Fermi sources. The same is valid for WR and Of stars, either in binary systems or isolated. OB associations are large systems that can contain more than a single gamma-ray source. We note that our study is based on two-dimensional coincidences, since we are comparing the equatorial coordinates of the sources.

2.3. Monte Carlo analysis

To determine the chance coincidences we used the Monte Carlo method for simulating sets of synthetic gamma-ray sources starting from the *Fermi* Large Area Telescope First Catalog. We followed a similar criteria to that used by Romero et al. (1999) to search for the possible association of unidentified *EGRET* sources with other type of celestial objects. In this algorithm, the galactic coordinates of a gamma-ray source (l, b) are moved to new ones (l', b'). The new galactic longitude coordinate is calculated by doing $l' = l + R_1 \times 360°$, where R_1 is a random number between 0 and 1 that never repeats from source to source or from set to set. Since the distribution of *Fermi* sources is almost constant in Galactic longitude, we do not impose any constraint on this coordinate in the simulations. The sources in the *Fermi* catalog have a given distribution in galactic latitude

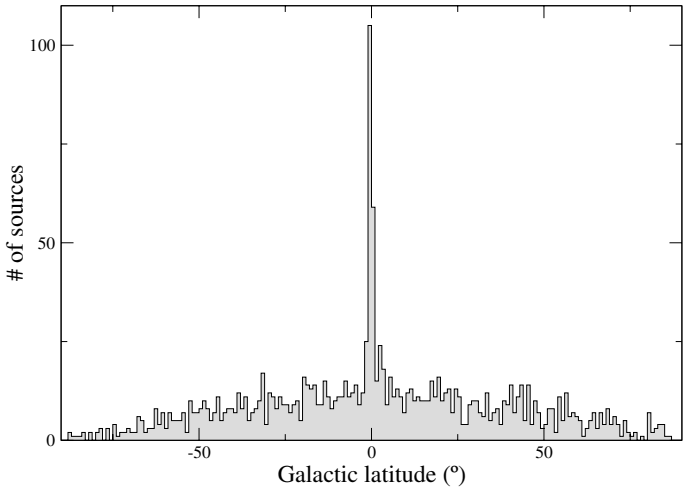

Fig. 1. Distribution of First *Fermi* Catalog sources in galactic latitude.

Table 1. List of the catalogs used in the study.

Object type	Catalog	# of sources
γ-ray sources	First *Fermi* Catalog[a]	1392[f]
YSO	RMS Survey[b]	637
WR	VIIth Catalog of Galactic Wolf-Rayet stars[c]	227
Of-type	A catalog of galactic O stars and the ionization of the low density interstellar medium by runaway stars[d]	664
OB associations	A new list of OB associations in our Galaxy[e]	88

Notes. [(a)] Abdo et al. (2010) , [(b)] Urquhart et al. (2008) , [(c)] van der Hucht (2001) , [(d)] Cruz-González et al. (1974) , [(e)] Mel'Nik & Efremov (1995) ; [(f)] number of gamma-ray sources after excluding the firm identifications.

(see Fig. 1). In order to constrain the simulations with this distribution, the galactic latitude coordinate is calculated by doing $b' = b + R_2 \times 1°$, where again R_2 is a random number between 0 and 1. Here, if the integer part of b' is greater than the integer part of b or the sign of b' is different than the sign of b, then b' is replaced by $b' - 1°$.

We simulated 1500 sets of synthetic *Fermi* sources and each set was compared with a fixed set of different kinds of objects: YSOs, WR stars, Of-type, and OB associations. In each simulation, we calculated the distance between the two sources using the statistical parameter S.

For each kind of compared objects we calculated the average number of coincidences and its standard deviation after all Monte Carlo simulations. We calculated the chance coincidence probability using the actual number of coincidences for each type of object and assuming a Gaussian distribution in the simulations. This probability allows us to know the reliability of our study. We also repeated this process moving the *Fermi* sources in 2°-bins in galactic latitude, i.e. replacing the galactic latitude coordinate by $b' = b + R_2 \times 2°$. If the integer part of b' is greater than the integer part of b or the sign of b' is different than the sign of b, then b' is replaced by $b' - 2°$. This binning allows us to keep the initial distribution in galactic latitude as well.

Table 2. Statistical results obtained from simulations.

Object type	Coincident γ-ray sources	Simulated 1°-bin	Probability 1°-bin	Simulated 2°-bin	Probability 2°-bin
YSO	12	4.4 ± 2.0	1.8×10^{-4}	3.6 ± 1.8	5.6×10^{-6}
WR	2	1.3 ± 1.1	2.9×10^{-1}	1.2 ± 1.1	2.9×10^{-1}
Of-type	5	2.9 ± 1.7	1.1×10^{-1}	2.9 ± 1.7	1.1×10^{-1}
OB assoc.	107	72.5 ± 8.0	4.2×10^{-6}	72.8 ± 8.0	5.5×10^{-6}

Notes. Latitude galactic coordinate has been constrained, while galactic longitude remains free.

3. Results

The results from our statistical study are shown in Table 2. In this table we list, from left to right, the object type, the number of coincidences between the each compared catalog and the original *Fermi* catalog, the simulated average number of coincidences, and the chance coincidence probability for each binning in galactic latitude. We find 12 gamma-ray sources spatially coincident with YSOs, 2 with WR stars, 5 with Of-type stars and 107 with OB associations.

From the Monte Carlo analysis, we see that there is a strong correlation between gamma-ray sources and YSOs: the catalog cross-check returns 12 coincidences between gamma-ray sources and YSOs. The Monte Carlo simulations, for the case of displacing the *Fermi* sources in 1°-bins, returns an average of coincidences of 4.4 ± 2.2 sources, which is the number of chance coincidences. This means that 7.6 of the 12 coincident *Fermi* sources (~63% of the total coincidences with a $\sim 4\sigma$ confidence level) should be associated with a probability of chance coincidence of 1.8×10^{-4}. Similarly, for displacing the *Fermi* sources in 2°-bins, we obtain an average of coincidences of 3.6 ± 1.8. That result indicates that 8.4 of the 12 coincident sources (~70% of the total coincidences with a $\sim 5\sigma$ confidence level) should be associated with a probability of 5.6×10^{-6} of being chance coincidences. In a similar way, the association of *Fermi* sources with WR and Of-type stars is unclear since the number of actual coincidences and the results of the Monte Carlo simulations are too similar and thus the probability of chance coincidence is too high (0.29 and 0.11 for WR stars and Of-type stars, respectively). The results for WR and Of-type stars are different from those obtained by Romero et al. (1999) for *EGRET* sources. The probability of chance coincidences has increased while the number of candidates decreased in the case of WR stars. In the case of Of-type stars the probability of chance association has increased as the number of coincidences increased as well. The probability of chance coincidence with OB associations is as low as $\sim 10^{-6}$. In this case, however, the nature of the gamma-ray emission is not clear, as it is discussed in Sect. 3.3.

3.1. Young stellar objects

The association of gamma-ray sources and massive YSOs has been suggested in the last years after studying a reasonable scenario for the production of non thermal emission (Araudo et al. 2007). However, this is the first time that the study of YSOs as gamma-ray sources is carried out in a statistical way, taking advantage of the *Fermi* catalog.

The results of our cross-check, shown in Table 3, indicate that 12 gamma-ray sources are positionally coincident with 23 YSOs. In this table we present, from left to right, the *Fermi* source name, its J2000 equatorial coordinates, its positional uncertainty, the spectral γ-ray index, the energy flux

Table 3. Positional coincidence of *Fermi* sources with MYSOs.

Fermi Name (1FGL)	RA (°)	Dec (°)	95% Semi major axis (°)	Spectral index Γ ($F \propto E^{-\Gamma}$)	Flux($E > 100$ MeV) $\times 10^{-11}$ erg cm^{-2} s^{-1}	MSX name	RA (°)	Dec (°)	$\Delta\theta$ (°)	Distance* (kpc)	L_{bol}* ($\times 10^3\ L_\odot$)	Mass ($M_\odot$)
J0541.1+3542	85.2805	35.7091	0.1397	2.41 ± 0.13	1.6 ± 0.5	G173.6328+02.8064	85.27929	+35.82633	0.12	1.6[a]	4.8[d]	
						G173.6339+02.8218	85.29592	+35.83380	0.13	1.6[a]	3.2[e]	
						G173.6882+02.7222	85.22758	+35.73558	0.05	1.6[a]	–	
J0647.3+0031	101.8417	0.5289	0.2150	2.41 ± 0.11	1.9 ± 0.5	G212.0641−00.7395	101.80567	+0.43514	0.10	6.4[b]	25[f]	
J1256.9−6337	194.2474	−63.6212	0.1955	2.26 ± 0.12	4.9 ± 1.1	G303.5990−00.6524	194.35546	−63.51650	0.12	11.3[b]	8.3[f]	
J1315.0−6235	198.7635	−62.5971	0.1860	2.31 ± 0.12	6.9 ± 0.0	G305.4840+00.2248	198.40016	−62.53708	0.18	3.6[b]	3.8[f]	
J1651.5−4602	252.8831	−46.0340	0.2258	2.21 ± 0.07	13.9 ± 3.4	G339.8838−01.2588[1]	253.01942	−46.14267	0.14	2.6[b]	21.0[f]	
J1702.4−4147	255.6039	−41.7859	0.0800	2.39 ± 0.07	8.7 ± 2.0	G344.4257+00.0451B	255.53674	−41.78303	0.05	5.0[b]	15.0[f]	
						G344.4257+00.0451C	255.53587	−41.78617	0.05	5.0[b]	15.0[f]	
J1846.8−0233	281.7001	−2.5628	0.1262	2.21 ± 0.06	9.3 ± 2.3	G030.1981−00.1691	281.76274	−2.51003	0.08	7.4[b]	29.0[f]	
J1848.1−0145	282.0470	−1.7605	0.0859	2.23 ± 0.04	9.5 ± 3.2	G030.9726−00.1410	282.09178	−1.80842	0.07	5.7[b]	3.9[f]	1.9×10^3[g]
						G030.9959−00.0771	282.04516	−1,75808	0.0044	5.7[b]	5.1[f]	1.9×10^3[g]
J1853.1+0032	283.2884	0.5366	0.5207	2.18 ± 0.07	5.7 ± 1.7	G032.8205−00.3300	282.04436	−1.75703	0.34	5.1[b]	17.0[f]	
						G033.3891+00.1989	282.89092	+0.49750	0.40	5.1[b]	11.0[f]	
						G033.3933+00.0100	283.06109	+0.41528	0.26	6.8[b]	7.9[e]	
						G033.5237+00.0198	283.11179	+0.53569	0.34	6.8[b]	7.9[e]	
						G034.0126−00.2832	283.60437	+0.83239	0.43	13.3[b]	34.0[f]	
						G034.0500−00.2977	283.63454	+0.85914	0.47	13.3[b]	24.0[f]	
J1925.0+1720	291.2748	17.3485	0.1443	2.28 ± 0.12	2.4 ± 1.0	G052.2025+00.7217A	291.24933	+17.42169	0.08	10.2[b]	15.0[f]	
						G052.2078+00.6890	291.28553	+17.41317	0.07	10.2[b]	20.0[f]	
J1943.4+2340	295.8667	23.6815	0.1118	2.23 ± 0.11	2.6 ± 0.7	G059.7831+00.0648[2,3]	295.79680	+23.73433	0.08	2.2[a]	6.8[f]	840 and 190 [h]
J2040.0+4157	310.0154	41.9533	0.1970	2.66 ± 0.06	7.9 ± 1.2	G081.5168+00.1926	309.99066	+41.98739	0.04	1.7[c]	0.704[f]	

Notes. [(1)] Detected in radio at 8.6 GHz with integrated flux of 2.6 mJy. [(2)] Detected in radio at 8.6 GHz with integrated flux of 1.0 mJy. [(3)] Observed in the X-ray with *Chandra* (Beuther et al. 2002a). Distances: [(a)] distance to the complex, taken from the literature; [(b)] kinematic distance determined from the systemic velocity of the complex, [(c)] distance has been taken from the literature; Luminosities: [(d)] *IRAS* fluxes; [(e)] *MSX* 21 μm band flux using a scaling relationship determined from a comparison with sources where spectral energy distribution (SED) fits have been possible; [(f)] SED fit to the available infrared fluxes (*2MASS, MSX, MIPSGAL/IGA*) and literature (sub)millimetre fluxes; [(*)] Data obtained from `http://www.ast.leeds.ac.uk/cgi-bin/RMS/RMS_DATABASE.cgi`; Masses: [(g)] from Ragan et al. (2006); [(h)] mass of the 2 cores identified in Beuther et al. (2002b) .

($E > 100$ MeV), the YSO name, its J2000 equatorial coordinates, the angular distance between the two compared sources, the distance to the YSO, its IR luminosity, and the mass of the star forming region where it is embedded.

In what follows we present a case by case discussion of the gamma-ray fields.

- 1FGL J0541.1+3542. This source is coincident with three YSOs: G173.6328+02.8604, G173.6339+02.8218 and G173.6882+02.7222. Their luminosities are below $4.8 \times 10^4\ L_\odot$. The three objects belong to the G173.6036+02.6237 complex (in the RMS Survey notation), which is situated at a distance of 1.6 kpc. We also find two Herbig Haro like objects, GGD 5 and GGD 6 (Gyulbudaghian et al. 1978), within the error ellipse of the *Fermi* source. Outside the *Fermi* error box the complex also harbors three more YSOs and an HII region.
- 1FGL J0647.3+0031. The YSO G212.0641-00.7395 is the only coincidence with this source. Its kinematic distance is 6.4 kpc and it has a luminosity of $2.5 \times 10^4\ L_\odot$. This source belongs to the G211.9800-00.9710 complex, together with another YSO that lies outside the error box of the gamma-ray source.
- 1FGL J1256.9−6337. We find G303.5990-00.6524 within the error ellipse of this gamma-ray source. It is a YSO with a bolometric luminosity of $8.3 \times 10^3\ L_\odot$ and located at a kinematic distance of 11.3 kpc. It belongs to the G303.5670-00.6253 complex that also harbors an HII region.
- 1FGL J1315.0−6235. This source is coincident with G305.4840+00.2248, which is a YSO with a luminosity of $3.8 \times 10^3\ L_\odot$ and located at a distance of 3.6 kpc.
- 1FGL J1651.5-4602. The source G339.8838-01.2588 is coincident with this gamma-ray source. It is a YSO with a bolometric luminosity of $2.1 \times 10^4\ L_\odot$. It is located at 2.6 kpc from the Earth. This source has been detected in radio at 8.6 GHz with an integrated flux of 2.6 mJy (Walsh et al. 1998). There is no indication of whether the radio flux is non thermal or not.
- 1FGL J1702.4−4147. This source is coincident with two YSOs: G344.4257+00451B and G344.4257+00451C, which form the G344.4120+00.0492 complex, together with two HII regions. They are located at 5 kpc from the Earth and both have a bolometric luminosity of $1.5 \times 10^4\ L_\odot$. These gamma-ray source is also near to a cluster of stars (see Dutra et al. 2003) and a molecular cloud (see Russeil & Castets 2004).
- 1FGL J1846.8−0233. We find a coincidence with the source G030.1981-00.1691. It has a bolometric luminosity of

2.9×10^4 $L_\odot$ and is located at 7.4 kpc. Within the error ellipse of the *Fermi* source, there are several other sources, such as dark nebulae and HII regions.

– 1FGL J1848.1−0145. This source is coincident with two YSOs, G030.9726-00.1410 and G030.9959-00.0771, located at 5.7 kpc and with bolometric luminosities of 3.9×10^3 $L_\odot$ and 5.1×10^3 $L_\odot$, respectively. Both are part of the G031.1451+00.0383 complex, which hosts five more YSOs (outside the *Fermi* error box), five diffuse HII regions, and ten HII regions. Within the error ellipse of the gamma-ray emission, there is an unidentified very high-energy gamma-ray source, HESS J1848-018 (Chaves et al. 2008), which is probably the most suitable very high-energy candidate counterpart to the *Fermi* detection.
– 1FGL J1853.1+0032. This source has the biggest error ellipse ($\Delta\theta_{95\%} \sim 0.5°$). For that reason, there is a high number of sources within its location error box, including pulsars, supernova remnants and X-ray sources. The cross-match of the catalogs yields six coincidences. These six YSOs belong to three different complexes with different distance to the Earth: G032.8205-00.3300 and G033.3891+00.1989 belong to the G033.1844-00.0572 complex, located at 5.1 kpc. The luminosities of these two sources are 1.7 and 1.1×10^3 $L_\odot$, respectively; G033.3933+00.0100 and G33.5237+00.0198 belong to the G033.6106+00.0464 complex, located at a distance of 6.8 kpc and the luminosity is 7.9×10^3 $L_\odot$ for both sources; G034.0126-00.2832 and G034.0500-00.2977 belong to the G034.0313-00.2904 complex. The distance to these objects is 13.3 kpc and their bolometric luminosities are 3.4×10^4 $L_\odot$ and 2.4×10^4 $L_\odot$, respectively.
– 1FGL J1925.0+1720. Two YSOs are coincident with it: G052.2025+00.7217A and G052.2078+00.6890. The bolometric luminosities are 1.5×10^4 $L_\odot$ and 2.0×10^4 $L_\odot$, respectively. They belong to the G052.2052+00.7053 complex which is located at 10.2 kpc, and hosts also a HII region.
– 1FGL J1943.4+2340. There is spatial coincidence with the source G059.7831+00.0648, located at 2.2 kpc. It has a bolometric luminosity of 6.8×10^4 $L_\odot$. This YSO has been detected in radio at 8.6 GHz with an integrated flux of 1.0 mJy (Sridharan et al. 2002). The infrared counterpart of this YSO is IRAS 19410+2336. It was observed by Chandra in 2002, which found hard X-ray emission from a number of sources within this high-mass star-forming region (Beuther et al. 2002a). The region has two cores where star formation takes place, with masses of 840 $M_\odot$ and 190 $M_\odot$ (Sridharan et al. 2002; Beuther et al. 2002b). In the latter paper, it is proposed that the X-ray emission is produced by magnetic reconnection effects between the protostars and their accretion disks. The interaction of several molecular outflows, where the YSO from the RMS survey is located, and the combined effects of the stellar winds make a good scenario that might result in particle acceleration up to relativistic energies.
– 1FGL J2040.0+4157. There is spatial coincidence with G081.5168+00.1926. This YSO is located at 1.7 kpc and shows a bolometric luminosity of 7.04×10^2 $L_\odot$. There is a galaxy (2MASX J20395796+4159152) located at 2.3″ from the position of that YSO.

3.2. WR and Of-type stars

We found two *Fermi* sources coincident with 15 WR stars in the Galactic center cluster and nine WR stars in the Quintuplet cluster. Some of these stars (see van der Hucht 2006) show variability and have been detected at X-rays with evidence of nonthermal emission. The results of our study are shown in Table 4. We cannot state that these two coincidences correspond to physical associations given the high chance association probability obtained from the Monte Carlo study. The first one is in the direction of the galactic center, and there are several other sources that introduce confusion. The second one was suggested as potential association with the Pistol Star in Abdo et al. (2010) and it is situated in a very crowded field.

In the case of Of-type stars, which are the evolved state of O stars, and precursors of WR stars, our results show that five *Fermi* sources are coincident with five stars (see Table 5). The probability of chance coincidence is too high to state a physical association. The sources 1FGL J1315.0-6235 and 1FGL J1853.1+0032 also show positional coincidence with YSOs (see Table 3). The case of association with YSOs has a much lower value for the chance probability. The source 1FGL J1112.1-6041 is coincident with HD 97434, a multiple star system. 1FGL J1315.0-6235 is located in a regions that harbors dark nebulae and molecular clouds. The Of star coincident with this source is HD 115071, which is a spectroscopic binary. Finally, 1FGL J2004.7+3343 is coincident with HD 227465, and there is also the source G70.7+1.2 inside the error box of the *Fermi* detection, which might contain a Be star and an X-ray-emitting B star pulsar binary (Cameron & Kulkarni 2007).

3.3. OB associations

Our study yields 107 *Fermi* sources positionally coincident with 35 OB associations, which represent ∼41% of the sample. We list the results in Table 6. We get this large number of gamma-ray sources because of the size of the OB associations. Most of them have angular sizes of ∼1° in diameter or higher. Our results extend those of Romero et al. (1999), where they found 26 coincidences between *EGRET* sources and OB associations. Most of the OB associations that they found are present in our results, along with other new candidates, as expected from the higher sensitivity of *LAT*. Although the number of sources has increased, the probability of chance associations is approximately the same as in Romero et al. (1999).

Most of the OB associations have fewer than five *Fermi* sources within their error boxes. There are seven OB associations with five or more *Fermi* sources within their error boxes. There are four associations with a number of gamma-ray coincidences between five and ten (Ori 1 B, Ori 1 C, Car 2, and Cyg 1, 8, 9), located at short distances from the Earth (less than 1 kpc) and located at galactic latitudes of ∼|15°| (association centroid position). There is an exception, Car 2, which is located at 2.2 kpc and has a galactic latitude of −0.13°. The OB associations with the large number of gamma-ray coincidences (>10) are those from Scorpius (Sco 2 A, Sco 2 B and Sco 2 D). Those associations are located at ∼170 pc on average and have very large angular sizes (∼9.5° on average).

There are five *Fermi* sources that are coincident with OB associations and YSOs at the same time: 1FGL J1256.9-6337, 1FGL J1315.5-6235, 1FGL J1702.4-447, 1FGL J1943.4+2340, and 1FGL J2040.0+4157. In all cases the OB association overlaps both the *Fermi* source and the YSO. In all cases but one, however, the distances to the YSO and the OB association are much too different.

4. Discussion

The fact that there are five *Fermi* sources coincident with both YSOs and OB associations makes us consider which is the

Table 4. Positional coincidence of *Fermi* sources with WR stars.

Fermi name (1FGL)	RA (°)	Dec (°)	95% Semi major axis (°)	Γ ($F \propto E^{-\Gamma}$)	Flux($E > 100$ MeV) $\times 10^{-10}$ erg cm^{-2} s^{-1}	Star	RA (°)	Dec (°)	$\Delta\theta$ (°)	Distance (kpc)
J1745.6-2900	266.420	−29.014	0.019	2.26 ± 0.03	7.1 ± 0.7	WR 101a[1]	266.41454	−29.00950	0.01	8.0
J1746.4-2849	266.618	−28.818	0.10	2.2 ± 0.5	4.6 ± 0.0	WR 102c[2]	266.54667	−28.81822	0.06	8.0

Notes. [(1)] WR stars 101 b, c, d, e, f, g, h, i, j, k, l, m, n, o, belonging to the Galactic Center Cluster lie at distances less than 20″ and are also within the error box of the gamma-ray source; [(2)] WR stars 102 d, e, f, g, h, i, j, k belonging to the Quintuplet Cluster lie at distances less than 1′ and are also coincident with the gamma-ray source.

Table 5. Positional coincidence of *Fermi* sources with Of stars.

Fermi name (1FGL)	RA (°)	Dec (°)	95% Semi major axis (°)	Γ ($F \propto E^{-\Gamma}$)	Flux($E > 100$ MeV) $\times 10^{-12}$ erg cm^{-2} s^{-1}	Star	RA (°)	Dec (°)	$\Delta\theta$ (°)	Distance[1] (kpc)
J0005.1+6829	1.2841	68.4883	0.4427	2.58 ± 0.12	1.7 ± 0.5	BD+67 1598	1.225	68.167	0.32	1.07
J1112.1-6041	168.0486	−60.6929	0.0461	2.12 ± 0.05	14.1 ± 1.6	HD 97434	167.975	−60.683	0.04	2.67
J1315.0-6235	198.7644	−62.5971	0.1860	2.31 ± 0.12	6.9 ± 0.0	HD 115071	199.000	−62.583	0.11	0.74
J1853.1+0032	283.2887	0.5369	0.5207	2.18 ± 0.07	5.7 ± 1.7	BD-0 3584	283.400	0.567	0.12	2.18
J2004.7+3343	301.1855	33.7171	0.1320	2.28 ± 0.08	5.2 ± 0.8	HD 227465	301.125	33.700	0.05	3.48

Notes. [(1)] Distances from Cruz-González et al. (1974).

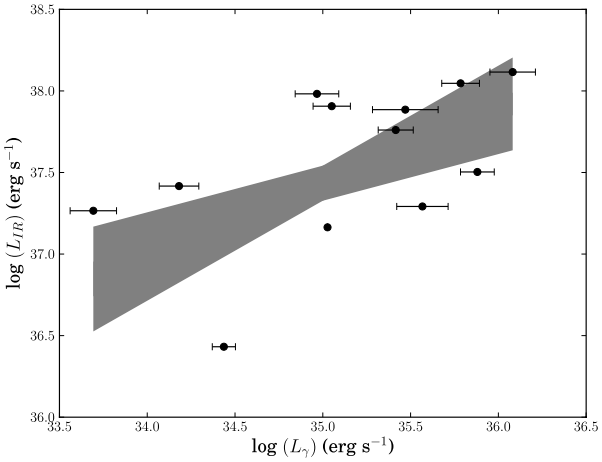

Fig. 2. IR luminosity versus gamma-ray luminosity above 100 MeV of the brightest YSOs coincident with each *Fermi* source. The shaded area represents the 1-σ confidence interval of a least square fit taking eight data points randomly and repeating the fit one thousand times. It can be roughly seen that the higher the gamma-ray luminosity, the higher the IR luminosity.

chance probability of having coincidence of *Fermi* sources with YSOs alone. Using the Monte Carlo algorithm again, but taking this constrain into account, we obtain a mean value of coincidences of 2.8 ± 1.7, and the chance probability for the seven *Fermi* sources coincident only with YSOs is ∼1.6%.

The brightest IR YSOs have more molecular mass available for proton-proton collisions and Bremsstrahlung interactions than those that are faint. It is expected then that the brightest IR YSOs would show the highest gamma-ray luminosity. To test such a trend, we have plotted in Fig. 2 the IR luminosity versus the gamma-ray luminosity of the brightest YSOs coincident with each *Fermi* source. The gamma-ray luminosity was calculated from the gamma-ray flux (see Table 3) assuming that the distance to the gamma-ray source is equal to the distance to the corresponding YSO. We see that, under this assumption, there is a trend toward increasing the gamma-ray luminosity as the IR luminosity increases, too. This trend, however, is obtained using the whole data set, and according to the results from our Monte Carlo simulations, we should have four chance coincidences out of the 12 candidates. To see how this could affect the trend, we selected eight data points randomly and fitted them to a straight line by least squares. We repeated this process one thousand times, getting an average least square fit within one standard deviation. The limits of this fit are plotted in Fig. 2. The increasing trend in the data is visible, although with a significant dispersion. This is not surprising considering the broad approach.

The association of WR stars with gamma-ray sources has been discussed in the past by Kaul & Mitra (1997) and Romero et al. (1999). In both cases, the authors studied the positional coincidence between WR stars and unidentified EGRET sources. In the later work, they find that two WR stars are of special interest: WR 140 and WR 142. The first one is a binary system, composed of a WC 7 plus an O4-5 star where the region of collision of the winds seems to be a good place for particle acceleration and high energy emission. It should be mentioned, however, that WR 140 is a long-period binary with variability expected on time scales of years (Williams et al. 1987). In the second one, WR 142, the hard X-ray emission and fast wind may indicate a colliding wind shock that could be explained by a companion close to this star (Sokal et al. 2010). No companion, however, has been reported so far. In our work none of these mentioned WR stars appear to be coincident with any *Fermi* source. The poor statistical correlations found from the simulations does not allow us to be confident with any of the coincidences found. The case of Of-type stars is also unclear since the probability of chance association is high.

Finally, our results for the OB associations are not conclusive. We list the results in Table 6. The probability of chance coincidence is negligible ($\sim 10^{-6}$), but we do get several gamma-ray sources for each OB association. Thus, is very difficult to assign a specific counterpart to the gamma-ray emission.

5. Conclusions

We studied the two-dimensional coincidence between unidentified *Fermi* sources and catalogs of galactic young objects, such as YSOs, WR stars, Of stars, and OB associations. We have found a statistical correlation between gamma-ray sources and YSOs. The correlation with the early type stars with strong winds remain unclear, since the candidates are located in crowded fields with many other alternatives to the gamma-ray emission, and the probability of chance associations is high. In the case of OB associations, the probability of chance associations is negligible. However, we cannot assign a specific counterpart to the gamma-ray emission because of the high angular size of most of OB associations.

What we have presented here is the first statistical evidence for gamma-ray emission from massive YSOs.

Acknowledgements. The authors acknowledge support from the Spanish Ministerio de Ciencia e Innovación (MICINN) under grant AYA2010-21782-C03-01. G.E.R. also acknowledges support of PIP 0078 (CONICET).

References

Abdo, A. A., Ackermann, M., Ajello, M., et al. 2010, ApJS, 188, 405
Allington-Smith, J. R., Perryman, M. A. C., Longair, M. S., Gunn, J. E., & Westphal, J. A. 1982, MNRAS, 201, 331
Araudo, A. T., Romero, G. E., Bosch-Ramon, V., & Paredes, J. M. 2007, A&A, 476, 1289
Banerjee, R., & Pudritz, R. E. 2006, ApJ, 641, 949
Banerjee, R., & Pudritz, R. E. 2007, ApJ, 660, 479
Benaglia, P., & Romero, G. E. 2003, A&A, 399, 1121
Beuther, H., Kerp, J., Preibisch, T., Stanke, T., & Schilke, P. 2002a, A&A, 395, 169
Beuther, H., Schilke, P., Sridharan, T. K., et al. 2002b, A&A, 383, 892
Binns, W. R., Wiedenbeck, M. E., Arnould, M., et al. 2008, Nex Astron., Rev., 52, 427
Bosch-Ramon, V., Romero, G. E., Araudo, A. T., & Paredes, J. M. 2010, A&A, 511, A8
Cameron, P. B., & Kulkarni, S. R. 2007, ApJ, 665, L135
Carrasco-González, C., Rodríguez, L. F., Anglada, G., et al. 2010, Science, 330, 1209
Chaves, R. C. G., Renaud, M., Lemoine-Goumard, M., & Goret, P. 2008, in Am. Inst. Phys. Conf. Ser., 1085, ed. F. A. Aharonian, W. Hofmann, & F. Rieger, 372
Cruz-González, C., Recillas-Cruz, E., Costero, R., Peimbert, M., & Torres-Peimbert, S. 1974, Rev. Mex. Astron. Astrofis., 1, 211
Curiel, S., Rodriguez, L. F., Moran, J. M., & Canto, J. 1993, ApJ, 415, 191
Dutra, C. M., Bica, E., Soares, J., & Barbuy, B. 2003, A&A, 400, 533
Garay, G., & Lizano, S. 1999, PASP, 111, 1049
Garay, G., Brooks, K. J., Mardones, D., & Norris, R. P. 2003, ApJ, 587, 739
Gyulbudaghian, A. L., Glushkov, Y. I., & Denisyuk, E. K. 1978, ApJ, 224, L137
Kaul, R. K., & Mitra, A. K. 1997, in AIP Conf. Ser., Proceedings of the Fourth Compton Symposium, ed. C. D. Dermer, M. S. Strickman, & J. D. Kurfess, 410, 1271
Kuhn, M. A., Getman, K. V., Feigelson, E. D., et al. 2010, ApJ, 725, 2485
Martí, J., Rodriguez, L. F., & Reipurth, B. 1993, ApJ, 416, 208
Mel'Nik, A. M., & Efremov, Y. N. 1995, Astron. Lett., 21, 10
Ragan, S. E., Bergin, E. A., Plume, R., et al. 2006, ApJS, 166, 567
Reid, M. J., Argon, A. L., Masson, C. R., Menten, K. M., & Moran, J. M. 1995, ApJ, 443, 238
Reipurth, B., & Bally, J. 2001, ARA&A, 39, 403
Rodriguez, L. F., Curiel, S., Moran, J. M., et al. 1989, ApJ, 346, L85
Romero, G. E. 2008, in AIP Conf. Ser., 1085 ed. F. A. Aharonian, W. Hofmann, & F. Rieger, 97
Romero, G. E., Benaglia, P., & Torres, D. F. 1999, A&A, 348, 868
Russeil, D., & Castets, A. 2004, A&A, 417, 107
Sokal, K. R., Skinner, S. L., Zhekov, S. A., Güdel, M., & Schmutz, W. 2010, ApJ, 715, 1327
Sridharan, T. K., Beuther, H., Schilke, P., Menten, K. M., & Wyrowski, F. 2002, ApJ, 566, 931
Tavani, M., Sabatini, S., Pian, E., et al. 2009, ApJ, 698, L142
Torres, D. F., Domingo-Santamaría, E., & Romero, G. E. 2004, ApJ, 601, L75
Urquhart, J. S., Hoare, M. G., Lumsden, S. L., Oudmaijer, R. D., & Moore, T. J. T. 2008, in Massive Star Formation: Observations Confront Theory, ed. H. Beuther, H. Linz, & T. Henning, ASP Conf. Ser., 387, 381
van der Hucht, K. A. 2001, New Astron. Rev., 45, 135
van der Hucht, K. A. 2006, A&A, 458, 453
Voelk, H. J., & Forman, M. 1982, ApJ, 253, 188
Walsh, A. J., Burton, M. G., Hyland, A. R., & Robinson, G. 1998, MNRAS, 301, 640
Williams, P. M., van der Hucht, K. A., van der Woerd, H., Wamsteker, W. M., & Geballe, T. R. 1987, in Instabilities in Luminous Early Type Stars, ed. H. J. G. L. M. Lamers, & C. W. H. De Loore, Astrophys. Space Sci. Lib., 136, 221

Pages 8 to 10 are available in the electronic edition of the journal at http://www.aanda.org

Table 6. Positional coincidence of *Fermi* sources with OB associations.

Fermi name (1FGL)	RA (°)	Dec (°)	95% Semi Major Axis (°)	Γ ($F \propto E^{-\Gamma}$)	Flux($E > 100$ MeV) $\times 10^{-12}$ erg cm^{-2}s^{-1}	OB association	RA (°)	Dec (°)	Distance[1] (kpc)	$\Delta\theta$ (°)	OB Size[1] (°)
J0205.6+6449	31.4090	64.8286	–	2.36 ± 0.06	3.78 ± 0.60	CLUST 1	31.03140	64.70406	0.89	0.20	0.9
J0214.1+6020	33.5476	60.3446	0.1624	2.1 ± 0.2	1.95 ± 0.68	PER 1 B	33.47470	59.59772	1.60	0.75	0.8
J0521.6+0103	80.4230	1.0512	0.1077	2.1 ± 0.2	0.92 ± 0	ORI 1 B	83.30102	−0.39051	0.50	3.22	6.6
J0534.7-0531	83.6872	−5.5222	0.1035	2.37 ± 0.09	3.51 ± 0.58	ORI 1 B	83.30102	−0.39051	0.50	5.15	6.6
						ORI 1 C	83.86341	−5.53543	0.66	0.18	3.0
J0536.2-0607	84.0623	−6.1285	0.0857	2.42 ± 0.07	3.79 ± 0.40	ORI 1 B	83.30102	−0.39051	0.50	5.79	6.6
						ORI 1 C	83.86341	−5.53543	0.66	0.63	3.0
J0539.4-0400	84.8703	−4.0166	0.2809	2.5 ± 0.1	1.06 ± 0.45	ORI 1 B	83.30102	−0.39051	0.50	3.95	6.6
						ORI 1 C	83.86341	−5.53543	0.66	1.82	3.0
J0540.4-0737	85.1220	−7.6268	0.0999	2.2 ± 0.1	1.31 ± 0.45	ORI 1 C	83.86341	−5.53543	0.66	2.44	3.0
J0540.9-0547	85.2317	−5.7900	0.3870	2.4 ± 0.1	1.29 ± 0.45	ORI 1 B	83.30102	−0.39051	0.50	5.73	6.6
						ORI 1 C	83.86341	−5.53543	0.66	1.39	3.0
J0541.9-0204	85.4885	−2.0754	0.0791	2.3 ± 0.1	1.77 ± 0.47	ORI 1 B	83.30102	−0.39051	0.50	2.76	6.6
J0547.0+0020	86.7698	0.3362	0.1868	2.50 ± 0.09	1.61 ± 0.43	ORI 1 B	83.30102	−0.39051	0.50	3.54	6.6
J0636.0+0458	99.0050	4.9806	0.0724	2.3 ± 0.1	4.76 ± 0.75	MON 1 B	99.37146	4.81144	1.48	0.40	0.6
J0705.9-1051	106.4985	−10.8528	0.1715	2.5 ± 0.1	1.72 ± 0.75	CMA 1 A	106.03646	−11.01884	0.75	0.48	1.0
J0709.0-1116	107.2576	−11.2758	0.0942	1.3 ± 0.6	2.08 ± 0.66	CMA 1 B	107.10737	−12.28821	1.30	1.02	1.2
J0841.9-4620	130.4865	−46.3448	0.2748	1.99 ± 0.09	2.42 ± 0.68	VELA 1 A	129.95838	−45.96976	1.43	0.52	1.1
J0854.0-4632	133.5039	−46.5424	0.1569	2.10 ± 0.09	4.19 ± 1.23	VELA 1 B	132.76816	−45.93533	1.41	0.79	1.0
J1045.2-5942	161.3059	−59.7059	0.0231	2.14 ± 0.03	26.2 ± 1.60	CAR 1 E	161.24112	−59.73526	2.64	0.04	1.5
J1057.2-6026	164.3242	−60.4495	0.0779	2.25 ± 0.06	6.86 ± 1.43	CAR 1-2	164.67677	−60.20707	2.62	0.30	0.5
						CAR 2	167.12384	−60.51125	2.16	1.38	2.5
J1104.0-6047	166.0209	−60.7974	0.0633	2.27 ± 0.06	6.84 ± 2.59	CAR 2	167.12384	−60.51125	2.16	0.61	2.5
J1106.7-6150	166.6808	−61.8449	0.0649	2.3 ± 0.1	5.46 ± 1.29	CAR 2	167.12384	−60.51125	2.16	1.35	2.5
J1112.1-6041	168.0486	−60.6929	0.0461	2.12 ± 0.05	14.2 ± 1.60	CAR 2	167.12384	−60.51125	2.16	0.49	2.5
J1115.2-6124	168.8028	−61.4022	0.1037	2.25 ± 0.08	9.73 ± 0	CAR 2	167.12384	−60.51125	2.16	1.21	2.5
J1119.4-6127	169.8532	−61.4528	0.0576	2.15 ± 0.08	5.51 ± 1.66	CAR 2	167.12384	−60.51125	2.16	1.62	2.5
						NGC 3576	169.66457	−61.13154	2.58	0.33	0.3
J1124.6-5916	171.1632	−59.2720	–	2.36 ± 0.06	4.54 ± 0.79	CAR 2	167.12384	−60.51125	2.16	2.38	2.5
J1127.7-6244	171.9345	−62.7412	0.1243	2.2 ± 0.1	3.99 ± 1.43	CRU 1 A	172.81985	−63.46201	2.58	0.82	1.0
						SCO 2 A	188.20526	−61.74213	0.16	7.64	8.0
J1134.8-6055	173.7198	−60.9320	0.0634	2.35 ± 0.07	4.16 ± 1.01	SCO 2 A	188.20526	−61.74213	0.16	7.00	8.0
J1136.0-6226	174.0206	−62.4342	0.1073	2.2 ± 0.1	4.16 ± 1.09	SCO 2 A	188.20526	−61.74213	0.16	6.68	8.0
J1207.4-6239	181.8754	−62.6552	0.0719	2.35 ± 0.06	8.20 ± 1.08	SCO 2 A	188.20526	−61.74213	0.16	3.09	8.0
J1213.7-6240	183.4475	−62.6743	0.0988	2.29 ± 0.08	4.77 ± 1.34	SCO 2 A	188.20526	−61.74213	0.16	2.41	8.0
J1234.0-5736	188.5059	−57.6129	0.0826	2.0 ± 0.1	1.26 ± 0.53	SCO 2 A	188.20526	−61.74213	0.16	4.13	8.0
J1241.6-6240	190.4160	−62.6798	0.1885	2.51 ± 0.09	4.71 ± 1.04	SCO 2 A	188.20526	−61.74213	0.16	1.39	8.0
J1256.1-5922	194.0496	−59.3778	0.1363	2.2 ± 0.2	1.19 ± 0.50	SCO 2 A	188.20526	−61.74213	0.16	3.72	8.0
J1256.9-6337	194.2482	−63.6213	0.1954	2.2 ± 0.1	4.97 ± 1.13	SCO 2 A	188.20526	−61.74213	0.16	3.35	8.0
J1300.7-5547	195.1930	−55.7989	0.2962	2.8 ± 0.1	1.92 ± 0.49	SCO 2 A	188.20526	−61.74213	0.16	6.96	8.0
J1301.4-6245	195.3587	−62.7609	0.1266	2.29 ± 0.09	5.22 ± 1.94	SCO 2 A	188.20526	−61.74213	0.16	3.48	8.0
J1306.4-6038	196.6202	−60.6381	0.1336	2.2 ± 0.1	1.76 ± 0.67	SCO 2 A	188.20526	−61.74213	0.16	4.20	8.0
J1307.3-6701	196.8482	−67.0235	0.1657	2.6 ± 0.1	1.32 ± 0.50	SCO 2 A	188.20526	−61.74213	0.16	6.47	8.0
J1309.9-6229	197.4964	−62.4869	0.1471	2.2 ± 0.1	5.16 ± 1.48	SCO 2 A	188.20526	−61.74213	0.16	4.41	8.0
J1315.0-6235	198.7644	−62.5971	0.1860	2.3 ± 0.1	6.86 ± 0	SCO 2 A	188.20526	−61.74213	0.16	5.00	8.0
J1317.5-6318	199.3793	−63.3037	0.0685	2.1 ± 0.1	6.64 ± 0	SCO 2 A	188.20526	−61.74213	0.16	5.39	8.0
J1320.6-6258	200.1639	−62.9693	0.1976	2.3 ± 0.1	4.60 ± 1.42	SCO 2 A	188.20526	−61.74213	0.16	5.68	8.0

Table 6. continued.

Fermi name (1FGL)	RA (°)	Dec (°)	95% Semi Major Axis (°)	Γ ($F \propto E^{-\Gamma}$)	Flux($E > 100$ MeV) $\times 10^{-12}$ erg cm^{-2}s^{-1}	OB association	RA (°)	Dec (°)	Distance[1] (kpc)	$\Delta\theta$ (°)	OB Size[1] (°)
J1322.0-4515	200.5154	−45.2652	0.2206	2.8 ± 0.1	4.01 ± 0.52	SCO 2 B	211.14639	−44.22469	0.18	7.62	7.8
J1325.6-4300	201.4148	−43.0110	0.0796	2.71 ± 0.06	7.94 ± 0.58	SCO 2 B	211.14639	−44.22469	0.18	7.15	7.8
J1328.2-4729	202.0508	−47.4991	0.0986	2.1 ± 0.1	2.53 ± 0.51	SCO 2 B	211.14639	−44.22469	0.18	7.13	7.8
J1333.4-4036	203.3574	−40.6042	0.4217	2.7 ± 0.1	1.80 ± 0.40	SCO 2 B	211.14639	−44.22469	0.18	6.80	7.8
J1334.2-4448	203.5635	−44.8136	0.1873	2.4 ± 0.1	1.23 ± 0.46	SCO 2 B	211.14639	−44.22469	0.18	5.44	7.8
J1347.8-3751	206.9674	−37.8551	0.1517	2.7 ± 0.1	2.13 ± 0.39	SCO 2 B	211.14639	−44.22469	0.18	7.11	7.8
J1400.1-3743	210.0356	−37.7177	0.1705	1.9 ± 0.2	1.67 ± 0	SCO 2 B	211.14639	−44.22469	0.18	6.56	7.8
J1407.5-4256	211.8885	−42.9485	0.1592	2.1 ± 0.2	1.06 ± 0.39	SCO 2 B	211.14639	−44.22469	0.18	1.38	7.8
J1417.7-4407	214.4286	−44.1320	0.2160	2.3 ± 0.2	1.98 ± 0.45	SCO 2 B	211.14639	−44.22469	0.18	2.36	7.8
J1417.7-5030	214.4405	−50.5111	0.2019	2.6 ± 0.2	1.57 ± 0.50	SCO 2 B	211.14639	−44.22469	0.18	6.67	7.8
J1428.2-4204	217.0711	−42.0711	0.0982	2.31 ± 0.07	2.99 ± 0.42	SCO 2 B	211.14639	−44.22469	0.18	4.83	7.8
J1501.6-4204	225.4096	−42.0819	0.4820	2.9 ± 0.2	1.62 ± 0.42	SCO 2 C	228.91604	−42.39408	0.16	2.61	5.8
J1513.2-5904	228.3209	−59.0821	0.0723	1.6 ± 0.3	6.56 ± 0	PIS 20	229.83477	−60.14507	0.96	1.31	1.3
J1514.1-4745	228.5328	−47.7527	0.1479	2.3 ± 0.1	1.45 ± 0.49	SCO 2 C	228.91604	−42.39408	0.16	5.37	5.8
J1514.7-5917	228.6808	−59.2924	0.1121	1.6 ± 0.3	4.40 ± 0	PIS 20	229.83477	−60.14507	0.96	1.03	1.3
J1542.9-2559	235.7479	−25.9849	0.1772	2.4 ± 0.2	1.21 ± 0.39	SCO 2 D	243.54161	−23.91278	0.18	7.36	11.7
J1548.7-2250	237.1930	−22.8394	0.0732	2.0 ± 0.2	1.92 ± 0.47	SCO 2 D	243.54161	−23.91278	0.18	5.93	11.7
J1548.9-5509	237.2377	−55.1647	0.0942	2.36 ± 0.09	3.63 ± 0.11	NOR 1	238.67814	−54.75670	1.10	0.92	1.1
J1553.4-2425	238.3711	−24.4210	0.1813	2.4 ± 0.2	1.30 ± 0.44	SCO 2 D	243.54161	−23.91278	0.18	4.74	11.7
J1553.5-3116	238.3877	−31.2713	0.0718	1.7 ± 0.2	1.17 ± 0.39	SCO 2 D	243.54161	−23.91278	0.18	8.66	11.7
J1554.0-5345	238.5184	−53.7663	0.1074	2.24 ± 0.07	15.6 ± 1.63	NOR 1	238.67814	−54.75670	1.10	0.99	1.1
J1600.7-3055	240.1792	−30.9264	0.0973	1.8 ± 0.1	1.25 ± 0	SCO 2 D	243.54161	−23.91278	0.18	7.62	11.7
J1607.5-2030	241.9000	−20.5118	0.0681	2.3 ± 0.2	1.29 ± 0.42	SCO 2 D	243.54161	−23.91278	0.18	3.73	11.7
J1613.6-5100	243.4201	−51.0010	0.0661	2.20 ± 0.06	7.65 ± 2.34	R 103 B	243.67674	−51.07046	3.00	0.18	0.3
J1614.7-5138	243.6767	−51.6411	0.1434	2.15 ± 0.06	12.8 ± 1.91	R 103 A	244.40278	−51.81465	3.22	0.48	0.4
J1620.9-2731	245.2310	−27.5272	0.1896	2.4 ± 0.1	1.49 ± 0.48	SCO 2 D	243.54161	−23.91278	0.18	3.92	11.7
J1623.5-2345	245.8923	−23.7527	0.3570	2.3 ± 0.1	3.62 ± 0	SCO 2 D	243.54161	−23.91278	0.18	2.16	11.7
J1625.7-2524	246.4282	−25.4163	0.0677	2.36 ± 0.06	4.52 ± 1.02	SCO 2 D	243.54161	−23.91278	0.18	3.02	11.7
J1625.8-2429	246.4749	−24.4971	0.0888	2.25 ± 0.07	7.00 ± 1.02	SCO 2 D	243.54161	−23.91278	0.18	2.74	11.7
J1626.2-2956	246.5667	−29.9409	0.1656	2.4 ± 0.1	1.85 ± 0.47	SCO 2 D	243.54161	−23.91278	0.18	6.60	11.7
J1626.2-2038	246.5702	−20.6485	0.4539	2.5 ± 0.1	1.83 ± 0.49	SCO 2 D	243.54161	−23.91278	0.18	4.30	11.7
J1627.8-3204	246.9511	−32.0761	0.1646	2.1 ± 0.1	1.22 ± 0.37	SCO 2 D	243.54161	−23.91278	0.18	8.70	11.7
J1627.8-1711	246.9712	−17.1897	0.1481	2.2 ± 0.2	0.99 ± 0.41	SCO 2 D	243.54161	−23.91278	0.18	7.45	11.7
J1628.6-2419	247.1638	−24.3296	0.1817	2.1 ± 0.1	4.19 ± 0	SCO 2 D	243.54161	−23.91278	0.18	3.33	11.7
J1632.7-2431	248.1931	−24.5203	0.1713	2.3 ± 0.1	1.79 ± 0.63	SCO 2 D	243.54161	−23.91278	0.18	4.29	11.7
J1632.9-4802	248.2264	−48.0402	0.0527	2.17 ± 0.05	14.0 ± 2.85	ARA 1A A	249.78617	−48.95281	1.59	1.38	1.3
J1640.8-4634	250.2024	−46.5816	0.0969	2.32 ± 0.04	19.2 ± 3.08	NGC 6204	251.38377	−47.30858	1.94	1.09	1.5
J1645.0-2155	251.2549	−21.9319	0.1919	2.3 ± 0.1	1.43 ± 0.43	SCO 2 D	243.54161	−23.91278	0.18	7.38	11.7
J1648.4-4609	252.1112	−46.1599	0.0553	2.29 ± 0.05	15.9 ± 3.98	NGC 6204	251.38377	−47.30858	1.94	1.25	1.5
J1702.-4147	255.6043	−41.7857	0.1040	2.50 ± 0.07	4.07 ± 0.53	SCO 1	253.59121	−41.50018	1.92	1.53	1.9
J1715.2-3319	258.8207	−33.3323	0.1397	2.3 ± 0.1	3.11 ± 0	SCO 4	258.66248	−33.68906	1.23	0.38	1.2
J1717.9-3343	259.4985	−33.7269	0.0832	2.42 ± 0.05	6.88 ± 1.03	SCO 4	258.66248	−33.68906	1.23	0.70	1.2
J1732.3-3243	263.0869	−32.7293	0.1243	2.33 ± 0.05	13.9 ± 1.91	TR 27	263.17260	−32.92243	1.31	0.21	1.1
J1810.9-1905	272.7486	−19.0843	0.0878	2.26 ± 0.06	11.0 ± 1.42	SGR 4	273.93407	−18.92533	1.85	1.13	1.5
J1811.3-1959	272.8294	−19.9920	0.0985	2.1 ± 0.2	5.75 ± 0	SGR 7	273.41595	−20.64018	1.28	0.85	0.8
						SGR 4	273.93407	−18.92533	1.85	1.49	1.5
J1814.0-1736	273.5201	−17.6008	0.0470	2.34 ± 0.04	14.8 ± 1.69	SGR 4	273.93407	−18.92533	1.85	1.38	1.5
J1817.6-1651	274.4099	−16.8602	0.1466	2.30 ± 0.06	5.91 ± 2.77	SER 1 A	275.20333	−16.63491	1.50	0.79	0.9

Table 6. continued.

Fermi name (1FGL)	RA (°)	Dec (°)	95% Semi Major Axis (°)	Γ ($F \propto E^{-\Gamma}$)	Flux($E > 100$ MeV) $\times 10^{-12}$ erg cm^{-2}s^{-1}	OB association	RA (°)	Dec (°)	Distance[1] (kpc)	$\Delta\theta$ (°)	OB Size[1] (°)
J1818.7-1557	274.6776	−15.9591	0.1114	2.34 ± 0.07	12.4 ± 1.92	SER 1 A	275.20333	−16.63491	1.50	0.84	0.9
J1821.1-1425	275.2907	−14.4198	0.0837	2.26 ± 0.06	7.58 ± 2.34	SCT 3	276.31989	−14.33074	1.48	1.00	1.1
J1823.2-1336	275.8135	−13.6060	0.0738	2.12 ± 0.05	16.3 ± 2.77	SCT 3	276.31989	−14.33074	1.48	0.88	1.1
J1825.7-1410	276.4394	−14.1818	0.0553	1.1 ± 0.3	6.86 ± 2.29	SCT 3	276.31989	−14.33074	1.48	0.19	1.1
J1826.2-1450	276.5630	−14.8481	–	2.38 ± 0.03	28.7 ± 2.31	SCT 3	276.31989	−14.33074	1.48	0.57	1.1
J1943.4+2340	295.8670	23.6818	0.1118	2.2 ± 0.1	2.62 ± 0.67	VUL 4	296.49937	24.37678	1.21	0.90	1.0
J1948.6+2437	297.1532	24.6293	0.1326	2.2 ± 0.1	2.26 ± 0.68	VUL 4	296.49937	24.37678	1.21	0.65	1.0
J2015.7+3708	303.9291	37.1402	0.0400	2.26 ± 0.03	13.9 ± 1.37	CYG 1,8,9	305.03403	38.92113	1.37	1.98	4.9
J2020.0+4049	305.0036	40.8191	0.1014	2.12 ± 0.08	8.16 ± 3.01	CYG 1,8,9	305.03403	38.92113	1.37	1.90	4.9
J2021.5+4026	305.3817	40.4460	–	2.25 ± 0.01	97.2 ± 3.48	CYG 1,8,9	305.03403	38.92113	1.37	1.55	4.9
J2030.0+3641	307.5021	36.6844	0.0559	2.10 ± 0.07	3.42 ± 1.07	CYG 1,8,9	305.03403	38.92113	1.37	2.97	4.9
J2032.8+3928	308.2006	39.4703	0.2507	2.59 ± 0.07	5.12 ± 1.39	CYG 1,8,9	305.03403	38.92113	1.37	2.51	4.9
J2034.7+3639	308.6968	36.6512	0.1254	2.2 ± 0.1	2.30 ± 0.69	CYG 1,8,9	305.03403	38.92113	1.37	3.68	4.9
J2040.0+4157	310.0158	41.9536	0.1970	2.66 ± 0.06	7.92 ± 1.19	CYG 1,8,9	305.03403	38.92113	1.37	4.86	4.9
J2207.5+6440	331.8799	64.6720	0.1971	2.65 ± 0.08	4.14 ± 0.52	CEP 2 B	328.84072	61.71559	0.77	3.26	3.6
J2214.5+5949	333.6453	59.8288	0.1184	2.4 ± 0.1	2.23 ± 0.62	CEP 2 B	328.84072	61.71559	0.77	3.01 3.6	
J2243.4+4104	340.8659	41.0733	0.1923	2.6 ± 0.2	1.71 ± 0	LAC 1	339.37867	39.90053	0.63	1.63 1.7	
J2250.8+6336	342.7210	63.6153	0.0687	2.33 ± 0.07	3.39 ± 0.43	CEP 3	344.37054	62.90856	0.84	1.02 1.9	

Notes. [(1)] From Cruz-González et al. (1974).